PHYSICAL REVIEW B **81**, 235408 (2010)

Electronic decoupling of an epitaxial graphene monolayer by gold intercalation

Isabella Gierz,[1,*] Takayuki Suzuki,[1,†] R. Thomas Weitz,[1,‡] Dong Su Lee,[1] Benjamin Krauss,[1] Christian Riedl,[1] Ulrich Starke,[1] Hartmut Höchst,[2] Jurgen H. Smet,[1] Christian R. Ast,[1] and Klaus Kern[1,3]

[1]*Max-Planck-Institut für Festkörperforschung, D-70569 Stuttgart, Germany*

[2]*Synchrotron Radiation Center, University of Wisconsin–Madison, Stoughton, Wisconsin 53589, USA*

[3]*Institut de Physique de la Matière Condensée, Ecole Polytechnique Fédérale de Lausanne, CH-1015 Lausanne, Switzerland*

(Received 9 March 2010; revised manuscript received 4 May 2010; published 4 June 2010)

The application of graphene in electronic devices requires large-scale epitaxial growth. The presence of the substrate, however, usually reduces the charge-carrier mobility considerably. We show that it is possible to decouple the partially sp^3-hybridized first graphitic layer formed on the Si-terminated face of silicon carbide from the substrate by gold intercalation, leading to a completely sp^2-hybridized graphene layer with improved electronic properties.

DOI: 10.1103/PhysRevB.81.235408 PACS number(s): 73.22.Pr

Electrons in graphene—sp^2-bonded carbon atoms arranged in a honeycomb lattice—behave like massless Dirac particles and exhibit an extremely high carrier mobility.[1] So far, the only feasible route toward large-scale production of graphene is epitaxial growth on a substrate. The presence of the substrate will, however, influence the electronic properties of the graphene layer. To preserve its unique properties it is desirable to decouple the graphene layer from the substrate. Here we present a different approach for the growth of highly decoupled epitaxial graphene on a silicon-carbide substrate. By decoupling the strongly interacting, partially sp^3 hybridized first graphitic layer [commonly referred to as zero layer (ZL) (Ref. 2)] from the SiC(0001) substrate by gold intercalation, we obtain a completely sp^2-hybridized graphene layer with improved electronic properties as confirmed by angle-resolved photoemission spectroscopy (ARPES), low-energy electron diffraction (LEED), scanning tunneling microscopy (STM), and Raman spectroscopy.

There are essentially two ways for large-scale epitaxial growth of graphene on a substrate: by cracking organic molecules on catalytic metal surfaces[3–7] or by thermal graphitization of SiC.[2,8–11] Unfortunately, the presence of the substrate alters the electronic properties of the graphene layer on the surface and reduces the carrier mobility. Even though it has been shown that the graphene layer can be decoupled from a metallic substrate[6,12–14] the system remains unsuitable for device applications. This problem can be solved by decoupling the graphene layer from a semiconducting SiC substrate.[15]

On both the silicon- and the carbon-terminated face of a SiC substrate, graphene is commonly grown by thermal graphitization in ultrahigh vacuum (UHV). When annealing the substrate at elevated temperatures Si atoms leave the surface whereas the C atoms remain and form carbon layers. On SiC(000$\bar{1}$), the so-called C face, the weak graphene-to-substrate interaction results in the growth of rotationally disordered multilayer graphene and a precise thickness control becomes difficult.[16] On the other hand, the rotational disorder decouples the graphene layers so that the transport properties resemble those of isolated graphene sheets with room-temperature mobilities in excess of 200 000 $cm^2/V\,s$.[17]

We have grown graphene on SiC(0001), i.e., the Si face, where the comparatively strong graphene-to-substrate interaction results in uniform, long-range ordered layer-by-layer growth. Our 4H-SiC wafers were hydrogen etched before insertion into UHV. To remove residual oxygen impurities we deposited Si from a commercial electron-beam evaporator at a substrate temperature of 800 °C until a sharp (3×3) LEED pattern was observed. We graphitized the samples by direct current heating at elevated temperature. The sample temperature was measured with an optical pyrometer at an emissivity of 63%. An annealing temperature of 1100 °C for 5 min is sufficient for the formation of the first carbon monolayer (ML). Within this so-called ZL every third C atom forms a chemical bond to a Si atom in the layer below. Those Si atoms below the ZL that do not bind to the ZL have unsaturated dangling bonds (see structural model in Ref. 15). The partial sp^3 hybridization of the ZL prevents the formation of π bands and therefore the ZL has no graphene properties. This can be seen in the first panel of Fig. 1(a), where the experimental band structure of the ZL (black) measured by ARPES near the $\bar{K}$ point of the surface Brillouin zone is shown. The measurements were done with a SPECS HSA 3500 hemispherical analyzer with an energy resolution of 10 meV and monochromatized He-II radiation at room temperature. The ZL lacks the linear dispersion typical for graphene π bands. Its band structure consists of two nondispersing bands at about −0.3 and −1.2 eV initial state energy. In addition, the ZL forms a $(6\sqrt{3}\times6\sqrt{3})R30°$ reconstruction with respect to the SiC substrate.[2,16,18,19]

Upon further annealing at 1150 °C for 5 min a purely sp^2-hybridized carbon layer forms on top of the ZL which shows the linear band-structure characteristic of massless charge carriers in graphene. The band structure of this "conventionally" grown graphene ML (cML) near the $\bar{K}$ point is shown in the second panel of Fig. 1(a). The cML is influenced considerably by the underlying SiC substrate. It is n doped with the crossing point of the two linear bands (Dirac point) at $E_D=-420$ meV due to charge transfer from the substrate.[8–10,15] Furthermore, the possibility of a band gap opening has been suggested[10] and explained theoretically in connection with the formation of midgap states.[20] In addition to that, the strong substrate influence reduces the carrier mo-

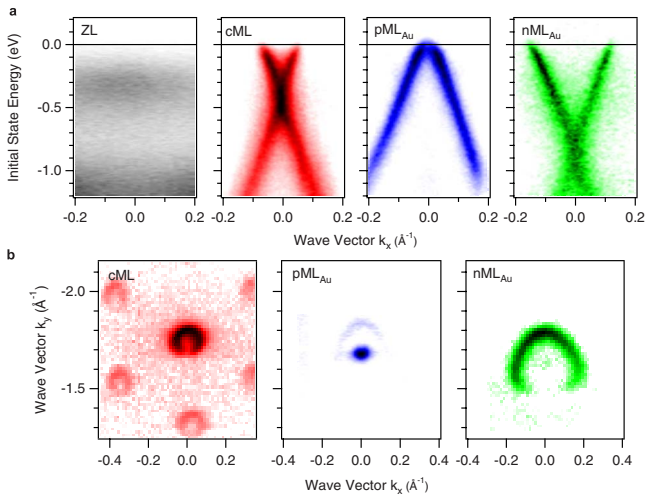

FIG. 1. (Color online) Comparison of ARPES data for conventional graphene on SiC and graphene intercalated with Au: panel (a) shows the band structure measured in the direction perpendicular to the $\overline{\Gamma K}$ direction near the $\bar{K}$ point of the surface Brillouin zone of the zero layer, the conventional graphene monolayer, the p-doped graphene monolayer intercalated with gold, and the n-doped graphene monolayer intercalated with gold together with the corresponding Fermi surfaces in panel (b). The Fermi surfaces are plotted on a logarithmic color scale to enhance weak features. The Fermi surfaces for the cML and the nML_{Au} were measured with a step size of 0.25° along the $\overline{\Gamma K}$ direction. As the linewidth for the pML_{Au} is narrower than for the cML and the nML_{Au} we had to reduce the stepsize to 0.1° to allow for reasonable accuracy. k_x is perpendicular to the $\overline{\Gamma K}$ direction, k_y is along the $\overline{\Gamma K}$ direction. The Fermi surface for the p-doped graphene monolayer shows a weak contribution of the n-doped phase due to an inhomogeneous Au coverage on the sample.

bility considerably.[21] The $(6\sqrt{3}\times 6\sqrt{3})R30°$ reconstruction of the ZL diffracts the outgoing photoelectrons giving rise to the formation of replica bands.[2] This is nicely seen in the measured Fermi surface of the cML around $\bar{K}$ in the left panel of Fig. 1(b). The Fermi-surface measurements were done at the Synchrotron Radiation Center (SRC) in Stoughton/Wisconsin using a Scienta analyzer with an energy resolution of better than 10 meV, a photon energy of $\hbar\omega$=52 eV and a sample temperature of 100 K. The angular resolution of 0.4° offers a momentum resolution of 0.023 Å^{-1} at the Fermi level. The size of the Fermi surface is determined by the charge-carrier density $n=k_F^2/\pi$, where k_F is the Fermi wave vector with respect to the $\bar{K}$ point. The values are summarized in Table I. The intensity distribution on the Fermi surface is not symmetric with respect to the $\bar{K}$ point. Only one of the two linearly dispersing π bands is visible along the $\overline{\Gamma K}$ direction (i.e., along k_y) because of interference effects in the photoemission process related to the two carbon atoms per unit cell.[22]

To reduce the influence of the substrate we developed a method for the epitaxial growth of graphene on the Si face of SiC. We start with the preparation of the ZL exploiting the strong substrate influence for uniform growth. On top of the ZL, we deposit Au atoms from a commercial Knudsen cell at room temperature. The gold coverage was callibrated using a quartz oscillator. After subsequent annealing of the sample at 800 °C the linear dispersion typical for graphene appears. Because graphitization of SiC only takes place for temperatures higher than 1000 °C we can exclude additional graphene growth at 800 °C. Depending on the gold coverage (about one-third or one monolayer, respectively), either a strongly n-doped (nML_{Au}) or a p-doped (pML_{Au}) graphene layer is formed. The band structures for the pML_{Au} and the nML_{Au} are compared in Fig. 1(a). In contrast to the ZL, both the pML_{Au} and the nML_{Au} clearly show two linearly dispersing π bands. The Dirac point for the pML_{Au} is about 100 meV above the Fermi level. This band structure looks similar to the one reported in Ref. 23. However, there the graphene monolayer was prepared by depositing Au directly on a cML and not on a ZL as in this work. For the nML_{Au} the bands cross at about −850 meV. The band structure of the cML is a superposition of the band structure of the underlying ZL and the graphene monolayer. Both pML_{Au} and nML_{Au}, however, are formed directly from the ZL. There is no additional carbon layer between the graphene layer and the substrate. Therefore, the band structure around the $\bar{K}$ point is given by pML_{Au} and nML_{Au} alone. The charge-carrier densities deduced from the size of the Fermi surface [see middle and right panels of Fig. 1(b)] are listed in Table I.

TABLE I. Characteristic parameters for cML, pML_{Au}, and nML_{Au} determined from the photoemission experiments.

	cML	pML_{Au}	nML_{Au}
Au coverage (ML)	0	1	1/3
Au-Si $4f_{5/2}$ (eV)		88.20	89.05
Au-Si $4f_{7/2}$ (eV)		84.54	85.41
Au-Au $4f_{5/2}$ (eV)		87.82	88.32
Au-Au $4f_{7/2}$ (eV)		84.15	84.68
Charge-carrier density (cm^{-2})	1×10^{13} electrons	7×10^{11} holes	5×10^{13} electrons
Dirac point (meV)	−420	+100	−850

Comparing the Fermi surfaces for the cML (red), the pML_{Au} (blue), and the nML_{Au} (green) in Fig. 1(b), the most striking difference is the absence of replica bands for pML_{Au} and nML_{Au}. Even on the logarithmic color scale of Fig. 1(b) the replica bands are invisible, indicating a reduced influence of the $(6\sqrt{3}\times 6\sqrt{3})R30°$ reconstruction.

This finding is supported by LEED images shown in Fig. 2. The LEED images were recorded at 126 eV electron energy because this energy is particularly sensitive to the graphene coverage.[24] The image for the cML shows the graphene (10) spot surrounded by satellite peaks from the $(6\sqrt{3}\times 6\sqrt{3})R30°$ reconstruction. The graphene (10) spot and the two left lower satellite spots have roughly the same intensity. For the ZL there is no graphene spot visible, only the satellite spots are there. The pML_{Au} has a very bright graphene spot, whereas the satellite peaks are considerably reduced in intensity. Furthermore, the distance between the satellite peaks and the graphene peak is smaller than for the cML indicating a larger lattice constant of the superstructure.

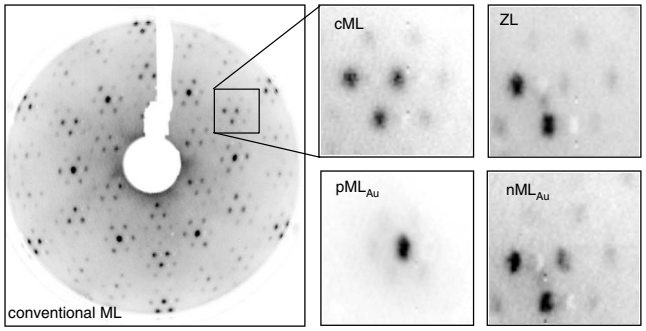

FIG. 2. LEED images taken at 126 eV for the cML, the ZL, the pML$_{Au}$, and the nML$_{Au}$. The relative intensity between graphene spot and satellite spots is a measure for the strength of the substrate influence on the graphene layer.

This can be related to an increase in the lattice constant in the pML$_{Au}$. The LEED image for the nML$_{Au}$ is very similar to that of the cML indicating a similar influence of the underlying substrate in both cases. We conclude that only the pML$_{Au}$ is less influenced by the underlying substrate. We attribute this to an increased graphene-to-substrate distance as will be discussed later in this paper.

To analyze the band structure in more detail and gain access to the relevant scattering mechanisms we determined the full width at half maximum (FWHM) of the bands by fitting momentum distribution curves along the $\overline{\Gamma K}$ direction with Lorentzian lineshapes and a constant background. The FWHM as a function of the initial state energy for the cML (red), the pML$_{Au}$ (blue), and the nML$_{Au}$ (green) are shown in Fig. 3(a). From the data in Fig. 3(a) a constant offset of 0.023 Å^{-1}(cML), 0.027 Å^{-1}(pML$_{Au}$), and 0.041 Å^{-1}(nML$_{Au}$) has been subtracted. For both cML and pML$_{Au}$ this offset is mainly determined by the experimental resolution. For the nML$_{Au}$, however, the linewidth offset is significantly larger than the limit set by the experimental resolution. In this case the offset is determined by impurity scattering which gives a constant contribution to the linewidth at all energies.

There are three main contributions to the quasiparticle lifetime in graphene.[2,8] The increase in linewidth around 200 meV is caused by electron-phonon coupling which depends on the size of the Fermi surface. Therefore, its influence is largest for strongly n-doped graphene, i.e. the nML$_{Au}$. The pronounced maximum near the Dirac point is attributed to electron-plasmon scattering. The third contribution to the linewidth is electron-electron scattering, which has been found to be proportional to $|E-E_F|^{\alpha}$, where $1<\alpha<2$.[8] The FWHM for our cML is in good agreement with the data reported in Refs. 2 and 8. Also, the cML and the nML$_{Au}$ have a similar linewidth. The main difference between the two is the position of the plasmon peak which is determined by the position of the Dirac point and hence the doping level. The pML$_{Au}$, however, has a much lower linewidth over the whole range of energies indicating a reduced electron-electron scattering. As the Fermi surface for the pML$_{Au}$ is rather small [see Fig. 1(b)] the electron-phonon contribution to the linewidth is negligible. The local maximum in linewidth around −1 eV initial state energy for the pML$_{Au}$ is not located at the Dirac point. Therefore, we do not interpret this as originating from plasmons within the graphene layer according to Refs. 2 and 8. Varykhalov *et al.*[6] found a similar feature for graphene/Au/Ni(111) which they attributed to an interaction between Au and graphene. The overall much smaller linewidth for the pML$_{Au}$ corroborates the conclusion from LEED that the pML$_{Au}$ is decoupled from the substrate. As mentioned before, the measured linewidth for the pML$_{Au}$ near the Fermi level is mainly determined by the experimental momentum resolution of $\Delta k=0.023$ Å^{-1}. This allows us to estimate a lower limit for the carrier lifetime using $\tau=\hbar/(\hbar v_F \Delta k)$. With $\hbar v_F=7.06$ eV Å, we find that $\tau \leq 4$ fs which is the same order of magnitude as the value reported for multilayer graphene on the C face of SiC.[17]

To gain a deeper insight into the structure of the pML$_{Au}$ and the nML$_{Au}$, we measured the Au 4*f* core-level spectra using a photon energy of 150 eV at the SRC. The data was fitted with Lorentzian peaks including a Shirley background. The spectra in Fig. 3(b) for the pML$_{Au}$ (blue) and the nML$_{Au}$

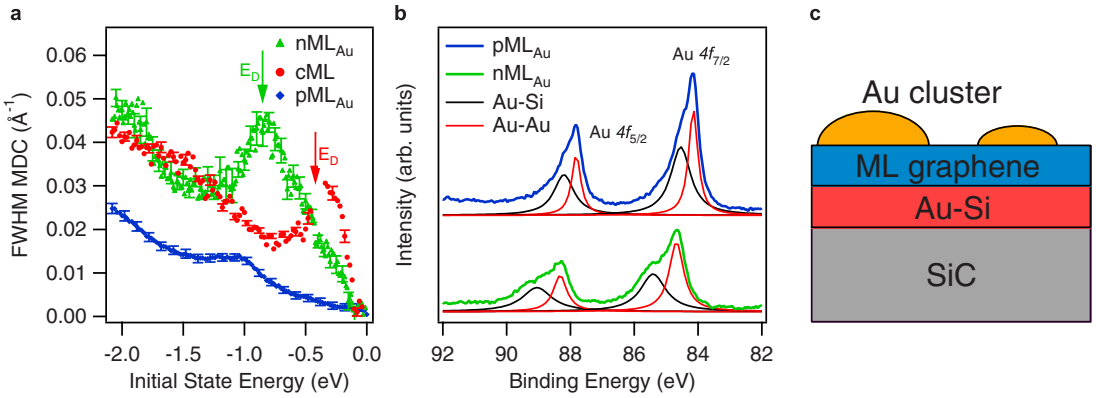

FIG. 3. (Color online) Linewidth analysis, Au 4*f* core-level spectra and schematic: panel (a) shows the FWHM of momentum distribution curves obtained from Fig. 1(a) for the conventional graphene monolayer (red), the p-doped graphene monolayer intercalated with Au (blue), and the n-doped graphene monolayer intercalated with Au (green). A constant background was subtracted from the data so that the plotted linewidth is determined by electron-phonon, electron-plasmon, and electron-electron scattering alone. Panel (b) shows the Au 4*f* core-level spectra recorded with an incident photon energy of 150 eV for the p-doped monolayer (blue) and the n-doped monolayer (green). The core-level spectra indicate the presence of Au-Si bonds (black lines) for both the p- and the n-doped monolayers which is consistent with the schematic (not to scale) shown in panel (c).

(green) show two different contributions to the Au 4*f* core level. The doublet at higher binding energy was attributed to a gold-silicide (Au-Si) configuration in earlier experiments with Au deposition on SiC(0001).[25,26] The doublet at lower binding energy belongs to Au-Au bonds.[27] The peak positions are summarized in Table I. The ratio between the integrated intensities for the gold-silicide doublet in the nML_{Au} and the pML_{Au} is Au-Si(nML_{Au}):Au-Si(pML_{Au})=0.39 indicating that the amount of gold-silicide in the pML_{Au} is roughly three times larger than in the nML_{Au}.

Combining these observations with the band structures in Fig. 1, we can deduce a schematic (not to scale) as depicted in Fig. 3(c). The appearance of a linear dispersion typical for graphene implies that the C-Si bonds between ZL and substrate break and a completely sp^2-hybridized carbon monolayer is created. The core-level spectra show the existence of gold-silicide for both the nML_{Au} and the pML_{Au}. We conclude that the Au atoms intercalate between the ZL and the substrate breaking the C-Si bonds to form gold-silicide. From the core-level peak intensity for the nML_{Au}, we find about one-third monolayer of Au intercalated (one monolayer corresponds to two Au atoms per graphene unit cell). We note that about every third carbon atom in the ZL forms a C-Si bond.[16] In view of the recovery of the sharp linear π-band structure this suggests that the intercalated gold sufficiently coordinates the Si atoms of the topmost SiC bilyer to completely suppress the covalent interface bonding. For the pML_{Au}, about one monolayer of gold is intercalated. From atomic force microscopy (AFM) and STM measurements (see Fig. 4), we find that additional Au atoms are not intercalated, but form Au clusters on top of the graphene layer which leads to the appearance of the Au-Au doublet in the Au 4*f* core levels. The ratio between the integrated intensities for the Au-Au and the Au-Si components is close to one for both pML_{Au} and nML_{Au}. Despite the fact that a complete monolayer of gold is intercalated for the pML_{Au} the substrate does not become metallic. Apart from the graphene bands, there are no other states visible at the Fermi energy.

The doping behavior for different Au coverages has been addressed by the theoretical work of Giovannetti *et al.*[28] who predicted p-type doping for graphene on a Au substrate. Reducing the Au-graphene distance to $d_{AuG}<3.2$ Å, however, will lead to n-type doping. The larger amount of intercalated Au for the pML_{Au} should increase the distance between graphene and substrate. This is consistent with the observed doping behavior as well as the reduced influence of the $(6\sqrt{3}\times 6\sqrt{3})R30°$ interface reconstruction on the Fermi surface and the LEED images of the pML_{Au}.

The peak position for the Au 4*f* doublet associated with gold-silicide shifts by about 860 meV from nML_{Au} to pML_{Au}. This can be related to the observed difference in the doping and a small change in the work function. The Au-Au component, on the other hand, shifts only by about 520 meV. We attribute the Au-Au bonds to Au clusters on top of the graphene layer. These clusters have an average height of a few nanometers [see Fig. 4(b)]. For such nanoparticles the position of the core levels depends rather sensitively on the size of the particle.[29,30] Thus, the shift of the Au-Au component of the Au 4*f* core level is most likely related to the size of the particular Au clusters.

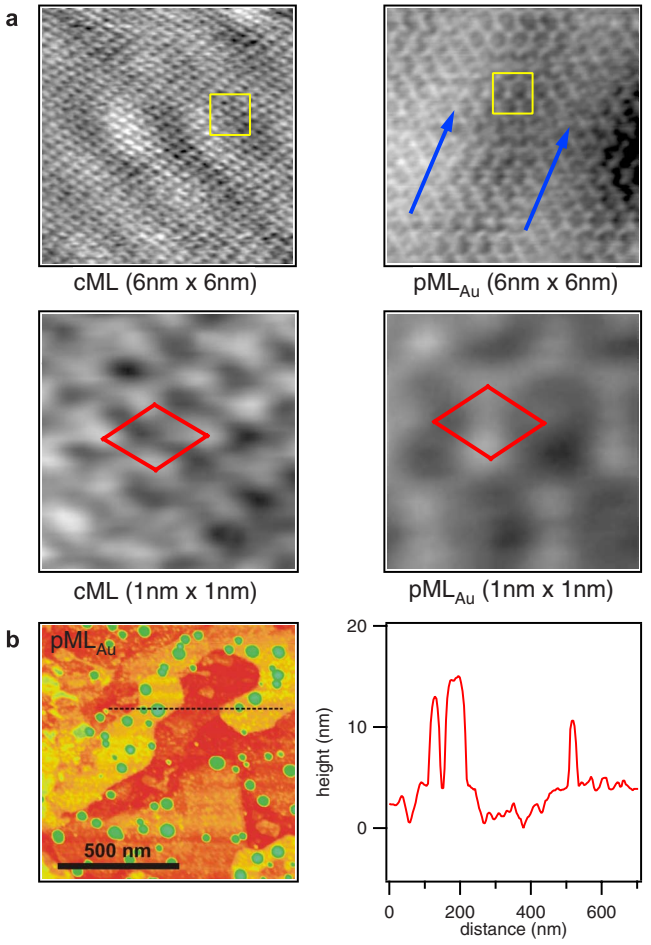

FIG. 4. (Color online) Panel (a) shows topographic STM images for the conventional graphene monolayer (left) and the p-doped graphene monolayer intercalated with Au (right). The lower panel shows a zoom in into the regions marked by a yellow square. The red diamond indicates the graphene unit cell. The images for the conventional monolayer and p-doped monolayer were recorded at a tunneling current of 0.2 nA and a bias of −0.5 V and −0.4 V, respectively. Panel (b) shows a large-scale AFM image for the p-doped graphene monolayer intercalated with Au together with a lineprofile extracted along the dashed line in the image. The AFM data clearly reveals the presence of Au clusters (green) on top of the graphene layer.

As both LEED and ARPES average over a rather large area on the sample surface, we used STM to gain access to the structure of the surface on an atomic scale. The images in Fig. 4(a) were measured with a room-temperature scanning tunneling microscope. The SiC samples with a ZL or cML on top were transferred to the STM chamber in air. Annealing of the samples at 800 °C was sufficient to remove any adsorbates from the surface. Au was deposited *in situ* from a commercial electron-beam evaporator. The images for the cML and the pML_{Au} were recorded at a tunneling current of 0.2 nA and a bias voltage of −0.5 V and −0.4 V, respectively. The upper panel of Fig. 4(a) shows topographic images of the cML and the pML_{Au} together with a zoom in of the area marked by a yellow square in the lower panel. The graphene unit cell is indicated by red lines. The cML shows a honey-

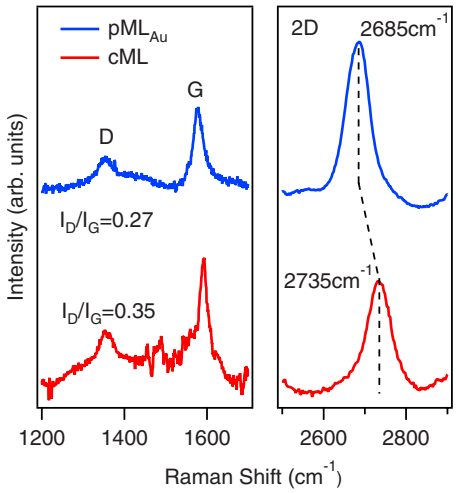

FIG. 5. (Color online) Comparison of the Raman scattering results for the conventional (red) and the p-doped (blue) graphene monolayers.

comb lattice with a $(6\sqrt{3}\times 6\sqrt{3})R30°$ modulation imposed by the ZL. The graphene lattice of the pML$_{Au}$ is well ordered and shows a superstructure of parallel stripes with a width of about 3 nm as marked by blue arrows. This superstructure could be of similar origin as the one reported in Ref. 31 despite the fact that the samples in Ref. 31 were prepared by depositing Au on a cML. The change in the lattice constant of the superstructure between cML and pML$_{Au}$ is also visible in LEED measurements in Fig. 2. Figure 4(b) shows a large-scale 1×1 μm^2 AFM image for the pML$_{Au}$ together with a lineprofile extracted along the dashed line in the image. The AFM data clearly reveals the presence of Au clusters (green) on top of the graphene layer. The gold clusters have a broad size distribution with a maximum height of about 15 nm.

To further investigate the degree of decoupling of the pML$_{Au}$, Fig. 5 shows Raman scattering data measured for the cML and the pML$_{Au}$. The Raman spectra were measured under ambient conditions using an argon-ion laser with a wavelength of 488 nm. The laser spot size was 400 nm in diameter and the laser power was 4 mW. The measured graphene signal is rather weak and superposed by the signal from the SiC substrate. We subtracted the substrate contribution so that the graphene peaks become clearly visible.[32] The Raman spectra are characterized by three main graphene contributions: The G peak corresponds to an in-plane vibration of the two sublattices with respect to each other. The D and the 2D peaks come from a double-resonance scattering process.[33] The 2D peak is always visible, whereas the D peak only appears in the presence of defects. Both G and 2D peaks shift as a function of doping[34–36] and strain.[37,38] Therefore, it is difficult to determine charge-carrier concentration and strain directly from the Raman data. However, the doping-induced shift is strongest for the G peak[35,36] whereas the effect of strain is more pronounced for the 2D peak.[37] If the effect of the charge-carrier concentration can be determined by another procedure (in this case ARPES data), the Raman data provide useful information about strain. The Raman spectrum for the ZL (not shown here) does not show any graphene-related features. The 2D peak of the pML$_{Au}$ (blue) appears at 2685 cm^{-1}. It is redshifted by 50 cm^{-1} as compared to the 2D peak of the cML. As the 2D peak position is only weakly dependent on charge doping,[35] we attribute the shift of the 2D peak to an increase in the lattice constant in agreement with the LEED data (see Fig. 3). The compressive strain present in the cML is apparently released in the pML$_{Au}$. This confirms the strongly reduced interactions observed in the analysis of the ARPES linewidth. The data in Fig. 5 also suggest that the D:G peak-intensity ratio has decreased for the pML$_{Au}$ (blue). As the D peak only exists in the presence of defects a reduced D:G peak-intensity ratio therefore indicates an improved crystalline quality.

We have shown that it is possible to decouple the graphene ZL formed on the Si face of SiC from the substrate by Au intercalation. This new slightly p-doped graphene has an improved quality and is only weakly influenced by the underlying substrate. Our ARPES measurements for the pML$_{Au}$ reveal a considerable reduction in linewidth. Our estimation for the carrier lifetime is of the same order of magnitude as the value for multilayer graphene on the C face of SiC. Therefore, we expect a considerable increase in carrier mobility for the pML$_{Au}$ and correspondingly the transport properties of our pML$_{Au}$ to be closer to those for multilayer graphene on the C face of SiC.

The authors thank C. L. Frewin, C. Locke, and S. E. Saddow of the University of South Florida for hydrogen etching of the SiC substrates. C.R.A. acknowledges funding by the Emmy-Noether-Program of the Deutsche Forschungsgemeinschaft (DFG). This work is based in part on research conducted at the Synchrotron Radiation Center of the University of Wisconsin-Madison which is funded by the National Science Foundation under Award No. DMR-0537588.

*Corresponding author; i.gierz@fkf.mpg.de
†Present address: Department of Electronics Engineering and Computer Science, Fukuoka University, Nanakuma 8-19-1, Jyonan, Fukuoka 814-0180, Japan.
‡Present address: Department of Physics, Harvard University, Cambridge, MA 02138, USA.

[1] A. K. Geim and K. S. Novoselov, Nature Mater. **6**, 183 (2007).
[2] A. Bostwick, T. Ohta, J. L. McChesney, K. V. Emtsev, T. Seyller, K. Horn, and E. Rotenberg, New J. Phys. **9**, 385 (2007).
[3] A. B. Preobrajenski, M. L. Ng, A. S. Vinogradov, and N. Mårtensson, Phys. Rev. B **78**, 073401 (2008).
[4] M. Sasaki, Y. Yamada, Y. Ogiwara, S. Yagyu, and S. Yamamoto, Phys. Rev. B **61**, 15653 (2000).
[5] I. Pletikosić, M. Kralj, P. Pervan, R. Brako, J. Coraux, A. T. N'Diaye, C. Busse, and T. Michely, Phys. Rev. Lett. **102**, 056808 (2009).

[6] A. Varykhalov, J. Sánchez-Barriga, A. M. Shikin, C. Biswas, E. Vescovo, A. Rybkin, D. Marchenko, and O. Rader, Phys. Rev. Lett. **101**, 157601 (2008).
[7] P. W. Sutter, J.-I. Flege, and E. Sutter, Nature Mater. **7**, 406 (2008).
[8] A. Bostwick, T. Ohta, T. Seyller, K. Horn, and E. Rotenberg, Nat. Phys. **3**, 36 (2007), and references therein.
[9] T. Ohta, A. Bostwick, T. Seyller, K. Horn, and E. Rotenberg, Science **313**, 951 (2006).
[10] S. Y. Zhou, G.-H. Gweon, A. V. Fedorov, P. N. First, W. A. de Heer, D.-H. Lee, F. Guinea, A. H. Castro Neto, and A. Lanzara, Nature Mater. **6**, 770 (2007).
[11] C. Berger, Z. Song, X. Li, X. Wu, N. Brown, C. Naud, D. Mayou, T. Li, J. Hass, A. N. Marchenkov, E. H. Conrad, P. N. First, and W. A. de Heer, Science **312**, 1191 (2006).
[12] A. M. Shikin, G. V. Prudnikova, V. K. Adamchuk, F. Moresco, and K.-H. Rieder, Phys. Rev. B **62**, 13202 (2000).
[13] D. Farías, A. M. Shikin, K.-H. Rieder, and Yu. S. Dedkov, J. Phys.: Condens. Matter **11**, 8453 (1999).
[14] Y. S. Dedkov, A. M. Shikin, V. K. Adamchuk, S. L. Molodtsov, C. Laubschat, A. Bauer, and G. Kaindl, Phys. Rev. B **64**, 035405 (2001).
[15] C. Riedl, C. Coletti, T. Iwasaki, A. A. Zakharov, and U. Starke, Phys. Rev. Lett. **103**, 246804 (2009).
[16] K. V. Emtsev, F. Speck, T. Seyller, L. Ley, and J. D. Riley, Phys. Rev. B **77**, 155303 (2008).
[17] M. Sprinkle, D. Siegel, Y. Hu, J. Hicks, A. Tejeda, A. Taleb-Ibrahimi, P. Le Fèvre, F. Bertran, S. Vizzini, H. Enriquez, S. Chiang, P. Soukiassian, C. Berger, W. A. de Heer, A. Lanzara, and E. H. Conrad, Phys. Rev. Lett. **103**, 226803 (2009).
[18] F. Varchon, R. Feng, J. Hass, X. Li, B. N. Nguyen, C. Naud, P. Mallet, J.-Y. Veuillen, C. Berger, E. H. Conrad, and L. Magaud, Phys. Rev. Lett. **99**, 126805 (2007).
[19] C. Riedl, U. Starke, J. Bernhardt, M. Franke, and K. Heinz, Phys. Rev. B **76**, 245406 (2007).
[20] S. Kim, J. Ihm, H. J. Choi, and Y.-W. Son, Phys. Rev. Lett. **100**, 176802 (2008).
[21] J. A. Robinson, M. Wetherington, J. L. Tedesco, P. M. Campbell, X. Weng, J. Stitt, M. A. Fanton, E. Frantz, D. Snyder, B. L. VanMil, G. G. Jernigan, R. L. Myers-Ward, C. R. Eddy, and D. K. Gaskill, Nano Lett. **9**, 2873 (2009).
[22] E. L. Shirley, L. J. Terminello, A. Santoni, and F. J. Himpsel, Phys. Rev. B **51**, 13614 (1995).
[23] I. Gierz, C. Riedl, U. Starke, C. R. Ast, and K. Kern, Nano Lett. **8**, 4603 (2008).
[24] C. Riedl, A. A. Zakharov, and U. Starke, Appl. Phys. Lett. **93**, 033106 (2008).
[25] C. Virojanadara and L. I. Johansson, Surf. Sci. **600**, 436 (2006).
[26] D. Stoltz, S. E. Stoltz, and L. S. O. Johansson, J. Phys.: Condens. Matter **19**, 266006 (2007).
[27] J. F. Moulder, W. F. Stickle, P. E. Sobol, and K. D. Bomben, *Handbook of X-ray Photoelectron Spectroscopy* (Physical Electronics, Minnesota, 1995).
[28] G. Giovannetti, P. A. Khomyakov, G. Brocks, V. M. Karpan, J. van den Brink, and P. J. Kelly, Phys. Rev. Lett. **101**, 026803 (2008).
[29] H.-G. Boyen, A. Ethirajan, G. Kästle, F. Weigl, P. Ziemann, G. Schmid, M. G. Garnier, M. Büttner, and P. Oelhafen, Phys. Rev. Lett. **94**, 016804 (2005).
[30] P. Torelli, L. Giordano, S. Benedetti, P. Luches, E. Annese, S. Valeri, and G. Pacchioni, J. Phys. Chem. C **113**, 19957 (2009).
[31] B. Premlal, M. Cranney, F. Vonau, D. Aubel, D. Casterman, M. M. De Souza, and L. Simon, Appl. Phys. Lett. **94**, 263115 (2009).
[32] D. S. Lee, C. Riedl, B. Krauss, K. von Klitzing, U. Starke, and J. H. Smet, Nano Lett. **8**, 4320 (2008).
[33] S. Reich and C. Thomsen, Philos. Trans. R. Soc. London, Ser. A **362**, 2271 (2004).
[34] S. Pisana, M. Lazzeri, C. Casiraghi, K. S. Novoselov, A. K. Geim, A. C. Ferrari, and F. Mauri, Nature Mater. **6**, 198 (2007).
[35] J. Yan, Y. B. Zhang, P. Kim, and A. Pinczuk, Phys. Rev. Lett. **98**, 166802 (2007).
[36] C. Stampfer, F. Molitor, D. Graf, K. Ensslin, A. Jungen, C. Hierold, and L. Wirtz, Appl. Phys. Lett. **91**, 241907 (2007).
[37] M. Huang, H. Yan, C. Chen, D. Song, T. F. Heinz, and J. Hone, Proc. Natl. Acad. Sci. U.S.A. **106**, 7304 (2009).
[38] Z. H. Ni, H. M. Wang, Y. Ma, J. Kasim, Y. H. Wu, and Z. X. Shen, ACS Nano **2**, 1033 (2008).